

---

# Adaptive Path-Integral Autoencoder: Representation Learning and Planning for Dynamical Systems

---

Jung-Su Ha, Young-Jin Park, Hyeok-Joo Chae, Soon-Seo Park, and Han-Lim Choi

Department of Aerospace Engineering, KAIST

Daejeon 305-701, Republic of Korea

{jsha, yjpark, hjchae, sspark}@lics., hanlimc@kaist.ac.kr

## Abstract

We present a representation learning algorithm that learns a low-dimensional latent dynamical system from high-dimensional *sequential* raw data, e.g., video. The framework builds upon recent advances in amortized inference methods that use both an inference network and a refinement procedure to output samples from a variational distribution given an observation sequence, and takes advantage of the duality between control and inference to approximately solve the intractable inference problem using the path integral control approach. The learned dynamical model can be used to predict and plan the future states; we also present the efficient planning method that exploits the learned low-dimensional latent dynamics. Numerical experiments show that the proposed path-integral control based variational inference method leads to tighter lower bounds in statistical model learning of sequential data. The supplementary video can be found at <https://youtu.be/NLM0GQ0o4jM>.

## 1 Introduction

Unsupervised learning of the underlying dynamics of sequential high-dimensional sensory inputs is the essence of intelligence because the learned dynamical model can be used to predict and plan the future state of the agent. Such learning problems are formulated as latent or generative model learning, which includes an intractable posterior inference of latent states for given input data. In the amortized variational inference framework, an inference network is introduced to output variational parameters of an approximate posterior distribution. This allows for a fast approximate inference procedure and efficient end-to-end training of the generative and inference networks when the learning signals from a loss function are back-propagated into the inference network with reparameterization trick [Kingma and Welling, 2014, Rezende et al., 2014]. The learning procedure is based on optimization of a surrogate loss, a low-bound of data likelihood, which results in two source of sub-optimality: an approximation gap and an amortization gap [Krishnan et al., 2018, Cremer et al., 2018]; the former comes from the sub-optimality of variational approximation (the gap between true posterior and optimal variational distribution) and the latter is caused by the amortized approximation (the gap between the optimal variational distribution and the distribution from the inference network). Recently, several works, e.g., [Hjelm et al., 2016, Krishnan et al., 2018, Kim et al., 2018], combined iterative refinement procedures to the amortized inference, where the output distribution of the inference network is used as a warm-start point of refinement. Since refined variational distributions do not rely only on the inference network, the sub-optimality from amortization gap can be mitigated and this technique is referred to as the *semi-amortized* inference.

For sequential data modeling, a generative model should be a dynamical system and a more sophisticated (approximate) inference method is necessary. If we assume the underlying dynamics has the Markov property, a state space model can be introduced, which allows the inference network

to be structured so as to mimic the factorized form of a true posterior distribution [Krishnan et al., 2017, Karl et al., 2017, Fraccaro et al., 2017]. The efficient end-to-end training with the amortized inference is also possible here, where the inference network should output the variational distribution of latent trajectories for given observation sequences. Even when the inference network is structure, the amortization gap increases inevitably because the inference should be performed in the trajectory space.

In this work, we present a semi-amortized variational inference method operated in the trajectory space. For a generative model given by a state space model, an initial state distribution and control inputs serve as parameters of variational distributions; the inference network outputs the initial states and the control input such that the corresponding latent trajectory well-describes the observation sequence. In this certain formulation, the divergence between the prior and the variational distribution is naturally derived from stochastic calculus. We observe that the inference problem in such a setting can be converted into a stochastic optimal control (SOC) problem, i.e., so-called control-inference duality [Todorov, 2008, Ruiz and Kappen, 2017]. In the SOC view, what the inference network does is to approximate the optimal control policy, which is hardly thought to be well-done when we observe that SOC problems are hard to solve at once, so iterative methods are generally used to solve the problems [Todorov, 2008, Tamar et al., 2016, Okada et al., 2017]. Thus, we adopt the adaptive path-integral control method to iteratively refine the variational parameters. We show that because samples from the refined variational distribution build tighter lower-bound and all the refinement procedures are fully differentiable, efficient end-to-end training is possible. Moreover, because the proposed framework is based on the SOC method, the same structure can be utilized to plan the future observation sequence, where the learned low-dimensional stochastic dynamics is used to explore the high-dimensional observation space efficiently.

## 2 Background

### 2.1 Statistical Modeling of Sequential Observations

Suppose that we have a set of observation sequences  $\{\mathbf{x}_{1:K}^{(i)}\}_{i=1,\dots,I}$ , where  $\mathbf{x}_{1:K}^{(i)} \equiv \{\mathbf{x}_k; \forall k = 1, \dots, K\}^{(i)}$  are i.i.d. sequences of observation that lie on (possibly high-dimensional) data space,  $\mathcal{X} \subset \mathbb{R}^{d_x}$ . The problem of interest is to build the probabilistic model that explains the data well. If the model is parameterized with  $\theta$ , the problem is formulated as the maximum likelihood estimation (MLE) problem:

$$\theta^* = \operatorname{argmax}_{\theta} \sum_i \log p_{\theta}(\mathbf{x}_{1:K}^{(i)}). \quad (1)$$

In this work, the observations are assumed to be emerged from the latent dynamical system, where a latent state trajectory,  $\mathbf{z}_{[0,T]} \equiv \{\mathbf{z}(t); \forall t \in [0, T]\}$ , lies on a (possibly low-dimensional) latent space,  $\mathcal{Z} \subset \mathbb{R}^{d_z}$ :

$$p_{\theta}(\mathbf{x}_{1:K}) = \int p_{\theta}(\mathbf{x}_{1:K} | \mathbf{z}_{[0,T]}) dp_{\theta}(\mathbf{z}_{[0,T]}), \quad (2)$$

where  $p_{\theta}(\mathbf{x}_{1:K} | \mathbf{z}_{[0,T]})$  and  $p_{\theta}(\mathbf{z}_{[0,T]})$  are called the conditional likelihood and the prior distribution, respectively<sup>1</sup>. In particular, we consider the state space model where latent states are governed by the continuous-time stochastic differential equation (SDE), i.e., the prior  $p_{\theta}(\mathbf{z}_{[0,T]})$  is a probability measure of a following system:

$$d\mathbf{z}(t) = \mathbf{f}(\mathbf{z}(t))dt + \sigma(\mathbf{z}(t))d\mathbf{w}(t), \quad \mathbf{z}(0) \sim p_0(\cdot), \quad (3)$$

where  $\mathbf{w}(t)$  is a  $d_u$ -dimensional Wiener process. Additionally, a conditional likelihood of a sequential observation is assumed to be factorized along the time axis:

$$p_{\theta}(\mathbf{x}_{1:K} | \mathbf{z}_{[0,T]}) = \prod_{k=1}^K p_{\theta}(\mathbf{x}_k | \mathbf{z}(t_k)), \quad (4)$$

where  $\{t_k\}$  is a sequence of discrete time points with  $t_1 = 0, t_K = T$ .

<sup>1</sup>Because each observation trajectory can be considered independently, we leave trajectory index,  $i$ , out and restrict our discussion to one trajectory for the sake of notational simplicity.

## 2.2 Amortized Variational Inference and Multi-Sample Objectives

The objective function (1) cannot be optimized directly because it contains the intractable integration. A surrogate loss function  $\mathcal{L}(q, \theta; \mathbf{x})$ , which is called the evidence lower bound (ELBO), is optimized alternatively:

$$\log p_\theta(\mathbf{x}) = \log \int p_\theta(\mathbf{x}|\mathbf{z})p_\theta(\mathbf{z})d\mathbf{z} \geq \mathbb{E}_{q(\mathbf{z})} \left[ \log \frac{p_\theta(\mathbf{x}|\mathbf{z})p_\theta(\mathbf{z})}{q(\mathbf{z})} \right] \equiv \mathcal{L}(q, \theta; \mathbf{x}), \quad (5)$$

where a variational distribution  $q(\cdot)$  can be any probabilistic distribution over  $\mathcal{Z}$  of which support includes that of  $p_\theta(\cdot)$ . The gap between the log-likelihood and the ELBO is the Kullback–Leibler (KL) divergence between  $q(\mathbf{z})$  and the posterior  $p_\theta(\mathbf{z}|\mathbf{x})$ :

$$\log p_\theta(\mathbf{x}) - \mathcal{L}(q, \theta; \mathbf{x}) = D_{KL}(q(\mathbf{z})||p_\theta(\mathbf{z}|\mathbf{x})). \quad (6)$$

To circumvent intractable posterior inference, the *amortized variational inference* approach can be taken, where the conditional variational distribution  $\mathbf{z} \sim q_\phi(\cdot|\mathbf{x})$  is introduced to approximate the intractable posterior distribution. In particular, the variational distribution  $q_\phi(\cdot|\mathbf{x})$ , which is referred as the *inference network*, is parameterized by  $\phi$ , so  $\theta$  and  $\phi$  can be simultaneously updated with  $\nabla_{(\theta, \phi)} \mathcal{L}(q_\phi, \theta; \mathbf{x})$  using the stochastic gradient ascent. Variational autoencoders (VAEs) [Kingma and Welling, 2014, Rezende et al., 2014] make  $q_\phi(\cdot|\mathbf{x})$  reparameterizable distribution, where  $\mathbf{z} = g_\phi(\mathbf{x}, \epsilon)$  is a differentiable deterministic function of an observation  $\mathbf{x}$  and  $\epsilon \sim d(\cdot)$  sampled from a known base distribution  $d(\cdot)$ . Then, the gradient can be estimated as:  $\nabla_{(\theta, \phi)} \mathcal{L}(q_\phi, \theta; \mathbf{x}) = \mathbb{E}_{d(\epsilon)} \left[ \nabla_{(\theta, \phi)} \log \frac{p_\theta(\mathbf{x}, g_\phi(\mathbf{x}, \epsilon))}{q_\phi(g_\phi(\mathbf{x}, \epsilon))} \right]$ , which generally yields a low variance estimator.

A tighter lower bound is achieved by using multiple samples,  $\mathbf{z}^{1:L}$ , independently sampled from  $q_\phi$ :

$$\mathcal{L}^L \equiv \mathbb{E}_{\mathbf{z}^{1:L} \sim q_\phi(\cdot|\mathbf{x})} \left[ \log \frac{1}{L} \sum_{l=1}^L \frac{p_\theta(\mathbf{x}, \mathbf{z}^l)}{q_\phi(\mathbf{z}^l|\mathbf{x})} \right]. \quad (7)$$

It is proven that, as  $L$  increases, the bounds gets tighter, i.e.,  $\log p_\theta(\mathbf{x}) \geq \dots \geq \mathcal{L}^{L+1} \geq \mathcal{L}^L \geq \dots$ , and the gap eventually vanishes [Burda et al., 2016, Cremer et al., 2017]. This multi-sample objective (7) is in the class of Monte Carlo objectives (MCO) in the sense that it utilizes independent samples to estimate the marginal likelihood [Mnih and Rezende, 2016],  $\hat{p}_\theta(\mathbf{x}) = \frac{1}{L} \sum_{l=1}^L \frac{p_\theta(\mathbf{x}, \mathbf{z}^l)}{q_\phi(\mathbf{z}^l|\mathbf{x})}$ ,  $\mathbf{z}^l \sim q_\phi(\cdot|\mathbf{x})$ . Defining  $w_{\theta, \phi}(\mathbf{x}, \mathbf{z}^l) \equiv \frac{p_\theta(\mathbf{x}, \mathbf{z}^l)}{q_\phi(\mathbf{z}^l|\mathbf{x})}$  and  $\tilde{w}^l \equiv \frac{w_{\theta, \phi}(\mathbf{x}, \mathbf{z}^l)}{\sum_i w_{\theta, \phi}(\mathbf{x}, \mathbf{z}^i)}$ , the gradient of (7) is given by:

$$\nabla_{(\theta, \phi)} \mathcal{L}^L = \mathbb{E}_{\epsilon^{1:L} \sim d(\cdot)} \left[ \sum_{l=1}^L \tilde{w}^l \nabla_{(\theta, \phi)} \log w_{\theta, \phi}(\mathbf{x}, g_\phi(\mathbf{x}, \epsilon^l)) \right]. \quad (8)$$

Since the parameter update is averaged over multiple samples with the weights  $\tilde{w}^l$ , the above procedure is referred as the importance weighted autoencoder (IWAE) [Burda et al., 2016]. The performance of IWAE’s training crucially depends on the variance of the importance weights  $\tilde{w}$  (or equivalently, on the effective sample size), which can be reduced by (i) increasing the number of samples and (ii) decreasing the gap between the proposal and the true posterior distribution; when the proposal  $q_\phi(\cdot|\mathbf{x})$  is equal to the true posterior  $p_\theta(\cdot|\mathbf{x})$ , the variance of the estimator reduces to 0, i.e.,  $\tilde{w}^l = 1/L$ .

## 2.3 Semi-Amortized Variational Inference with Iterative Refinement

As mentioned previously, the performance of generative model learning depends on the gap between the variational and the posterior distributions. Thus, the amortized inference has two sources of this gap: the approximation and amortization gaps [Krishnan et al., 2018, Cremer et al., 2018]. The approximation gap comes up by using the variational distribution to approximate the posterior distribution, which is given by the KL-divergence between the posterior distribution and the optimal variational distribution. The amortization gap is caused by the limit of the expressive power of inference networks, where the variational parameters are *not* individually optimized for each observation but amortized over entire observations. To address the issue of the amortization gap, a hybrid approach can be considered; for each observation, the variational distribution is refined individually from the output of the inference network. Compared to the amortized variational inference, this hybrid approach, coined semi-amortized variational inference, allows for utilizing better variational parameters in a model learning.

### 3 Path Integral Adaptation for Variational Inference

#### 3.1 Controlled SDE as variational distribution

When handling sequential observations, the variational distribution family should be carefully chosen so as to efficiently handle increasing dimensions of variables along the time-axis. In this work, the variational proposal distribution is given by the trajectory distribution of a controlled stochastic dynamical system, where the controls,  $\mathbf{u} \in \mathbb{R}^{d_u}$ , and parameters of an initial state distribution,  $q_0$ , serve as variational parameters, i.e., the proposal  $q_{\mathbf{u}}(\mathbf{z}_{[0,T]})$  is a probability measure of a following system:

$$d\mathbf{z}(t) = \mathbf{f}(\mathbf{z}(t))dt + \sigma(\mathbf{z}(t))(\mathbf{u}(t)dt + d\mathbf{w}(t)), \quad \mathbf{z}(0) \sim q_0(\cdot). \quad (9)$$

By applying Girsanov's theorem in Appendix A that provides the likelihood ratio between  $p(\mathbf{z}_{[0,T]})$  and  $q_{\mathbf{u}}(\mathbf{z}_{[0,T]})$ , the ELBO is written as:

$$\mathcal{L} = \mathbb{E}_{q_{\mathbf{u}}(\mathbf{z}_{[0,T]})} \left[ \log p_{\theta}(\mathbf{x}_{1:K} | \mathbf{z}_{[0,T]}) + \log \frac{p_0(\mathbf{z}(0))}{q_0(\mathbf{z}(0))} - \frac{1}{2} \int_0^T \|\mathbf{u}(t)\|^2 dt - \int_0^T \mathbf{u}(t)^T d\mathbf{w}(t) \right]. \quad (10)$$

Then, the problem of finding the optimal variational parameters  $\mathbf{u}^*$  and  $q_0^*$  (or equivalently, the best approximate posterior) can be formulated as a SOC problem:

$$\mathbf{u}^*, q_0^* = \underset{\mathbf{u}, q_0}{\operatorname{argmin}} \mathbb{E}_{q_{\mathbf{u}}(\mathbf{z}_{[0,T]})} \left[ V(\mathbf{z}_{[0,T]}) + \frac{1}{2} \int_0^T \|\mathbf{u}(t)\|^2 dt + \int_0^T \mathbf{u}(t)^T d\mathbf{w}(t) \right], \quad (\text{SOC})$$

where  $V(\mathbf{z}_{[0,T]}) \equiv -\log \frac{p_0(\mathbf{z}(0))}{q_0(\mathbf{z}(0))} - \sum_{k=1}^K \log p_{\theta}(\mathbf{x}_k | \mathbf{z}(t_k))$  serves as a state cost of the SOC problem.

Suppose that the control policy is discretized along the time-axis with the control parameters  $\{\mathbf{u}_k^{ff}, \mathbf{K}_k\}_{k=1, \dots, K-1}$  as  $\mathbf{u}(t, \mathbf{z}(t)) = \mathbf{u}_k^{ff} - \mathbf{K}_k \mathbf{z}(t)$ ,  $\forall t \in [t_k, t_{k+1})$ , and the initial distribution is assumed to be the Gaussian distribution,  $q_0(\cdot) = \mathcal{N}(\cdot; \hat{\mu}_0, \hat{\Sigma}_0)$ . Once the inference problem is converted into the SOC problem, the principle of optimality [Bellman, 2013] provides the sophisticated and efficient structure of inference networks. Note that, by the principle of optimality, the optimal initial state distribution depends on the cost for all time horizon  $[0, T]$  but the optimal control policy at  $t$  only relies on the future cost in  $(t, T]$ . Such a structure can be implemented using a backward recurrent neural network (RNN) to output the approximate optimal control policy; while the hidden states of the backward RNN compresses the information of a given observation sequence backward in time, the hidden state at each time step,  $k = K - 1, \dots, 2$ , outputs the control policy parameters,  $\{\mathbf{u}_k^{ff}, \mathbf{K}_k\}$ . Finally, the first hidden state additionally outputs the initial distribution parameters,  $\{\hat{\mu}_0, \hat{\Sigma}_0, \mathbf{u}_1^{ff}, \mathbf{K}_1\}$ . For the detailed descriptions and illustrations, see Fig. 3 and Algorithm 2 in Appendix C.

#### 3.2 Adaptive Path-Integral Autoencoder

(SOC) is in a class of linearly-solvable optimal control problems [Todorov, 2009] of which the objective function can be written as a KL-divergence form:

$$J = D_{KL}(q_{\mathbf{u}}(\mathbf{z}_{[0,T]}) || p^*(\mathbf{z}_{[0,T]})) - \log \xi, \quad (11)$$

where  $p^*$ , represented as  $dp^*(\mathbf{z}_{[0,T]}) = \exp(-V(\mathbf{z}_{[0,T]})) dp_{\theta}(\mathbf{z}_{[0,T]}) / \xi$ , is a probability measure induced by optimally-controlled trajectories and  $\xi \equiv \int \exp(-V(\mathbf{z}_{[0,T]})) dp_{\theta}(\mathbf{z}_{[0,T]})$  is a normalization constant (see Appendix A for details). By applying Girsanov's theorem again, the optimal trajectory distribution is expressed as:

$$dp^*(\mathbf{z}_{[0,T]}) \propto dq_{\mathbf{u}}(\mathbf{z}_{[0,T]}) \exp(-S_{\mathbf{u}}(\mathbf{z}_{[0,T]})), \quad (12)$$

$$S_{\mathbf{u}}(\mathbf{z}_{[0,T]}) = V(\mathbf{z}_{[0,T]}) + \frac{1}{2} \int_0^T \|\mathbf{u}(t)\|^2 dt + \int_0^T \mathbf{u}(t)^T d\mathbf{w}(t). \quad (13)$$

This implies that the optimal trajectory distribution can be approximated by sampling a set of trajectories according to the controlled dynamics with  $\mathbf{u}(t)$ , i.e.  $\mathbf{z}_{[0,T]}^l \sim q_{\mathbf{u}}(\cdot)$ , and assigning their

importance weights as  $\tilde{w}^l = \frac{\exp(-S_{\mathbf{u}}(\mathbf{z}_{[0,T]}^l))}{\sum_{i=1}^L \exp(-S_{\mathbf{u}}(\mathbf{z}_{[0,T]}^i))}$ ,  $\forall l \in \{1, \dots, L\}$ . Similar to the MCO's case, the variance of importance weights decreases as the control input  $\mathbf{u}(\cdot)$  gets closer to the true optimal control input  $\mathbf{u}^*(\cdot)$  and it reduces to 0 when  $\mathbf{u}(t) = \mathbf{u}^*(t, \mathbf{z}(t))$  [Thijssen and Kappen, 2015].

The path-Integral control is a sampling-based SOC method, which approximates the optimal trajectory distribution,  $\hat{p}^*$ , with weighted sample trajectories using (12)–(13) and updates control parameters based on moment matching of  $q_{\mathbf{u}}$  to  $\hat{p}^*$ . Suppose that  $\hat{p}^*$  is approximated using sample trajectories and assigning their weights,  $\{\mathbf{z}_{[0,T]}^l, \tilde{w}^l\}_{l=1, \dots, L}$ , as above and let  $\mathbf{u}^{ff}(t)$  and  $\mathbf{K}(t)$  represent feedforward control and feedback gain, respectively. This work considers a standardized linear feedback controller to regularize the first and second moments of trajectory distributions, where a control input has a form as:

$$\mathbf{u}(t) = \mathbf{u}^{ff}(t) + \mathbf{K}(t)\Sigma^{-1/2}(t)(\mathbf{z}(t) - \mu(t)), \quad (14)$$

where  $\mu(t) = \sum_{l=1}^L \tilde{w}^l \mathbf{z}^l(t)$  and  $\Sigma(t) = \sum_{l=1}^L \tilde{w}^l (\mathbf{z}^l(t) - \mu(t))(\mathbf{z}^l(t) - \mu(t))^T$  are the mean and covariance of the state w.r.t.  $\hat{p}^*$ , respectively. Suppose a new set of trajectories and their weights is obtained by a (previous) control policy  $\mathbf{u}(t) = \bar{\mathbf{u}}^{ff}(t) + \bar{\mathbf{K}}(t)\bar{\Sigma}^{-1/2}(t)(\mathbf{z}(t) - \bar{\mu}(t))$ . Then, the path integral control theorem in Appendix B gives the update rules with the adaptation rate  $\eta$  as:

$$\mathbf{u}^{ff}(t)dt = \bar{\mathbf{u}}^{ff}(t)dt + \bar{\mathbf{K}}(t)\bar{\Sigma}^{-1/2}(t)(\mu(t) - \bar{\mu}(t))dt + \eta \sum_{l=1}^L \tilde{w}^l d\mathbf{w}^l(t), \quad (15)$$

$$\mathbf{K}(t)dt = \bar{\mathbf{K}}(t)\bar{\Sigma}^{-1/2}(t)\Sigma^{1/2}(t)dt + \eta \sum_{l=1}^L \tilde{w}^l d\mathbf{w}^l(t) \left( \Sigma^{-1/2}(t)(\mathbf{z}^l(t) - \mu(t)) \right)^T. \quad (16)$$

In addition, the initial state distribution also can be updated into  $q_0(\cdot) = \mathcal{N}(\cdot; \hat{\mu}_0, \hat{\Sigma}_0)$ :

$$\hat{\mu}_0 = \sum_{l=1}^L \tilde{w}^l \mathbf{z}^l(0), \quad \hat{\Sigma}_0 = \sum_{l=1}^L \tilde{w}^l (\mathbf{z}^l(0) - \hat{\mu}_0)(\mathbf{z}^l(0) - \hat{\mu}_0)^T. \quad (17)$$

Starting from the variational parameters,  $\{\hat{\mu}_0, \hat{\Sigma}_0, \mathbf{u}_{1:K-1}^{ff}, \mathbf{K}_{1:K-1}\}$ , given by the inference network and  $\bar{\mu}(t) = 0, \bar{\Sigma}(t) = I$ , the update rules in (15)–(17) gradually refine the parameters of  $q_{\mathbf{u}}$  in order for the resulting trajectory distribution to be close to the posterior distribution. After  $R$  adaptations, the MCO and its gradient are estimated by:

$$\hat{\mathcal{L}}^L = \log \frac{1}{L} \sum_{l=1}^L \exp(-S_{\mathbf{u}}(\mathbf{z}_{[0,T]}^l)), \quad \nabla_{\theta, \phi} \hat{\mathcal{L}}^L = - \sum_{l=1}^L \tilde{w}^l \nabla_{\theta, \phi} S_{\mathbf{u}}(\mathbf{z}_{[0,T]}^l), \quad (18)$$

where  $\theta$  and  $\phi$  denote the parameters of the generative model, i.e.,  $\mathbf{f}(\mathbf{z}), \sigma(\mathbf{z}), p_0(\mathbf{z})$  and  $p(\mathbf{x}|\mathbf{z})$ , and the inference network, i.e., the backward RNN, respectively. Because all procedures in the path integral adaptation and MCO construction are differentiable, they can be implemented by a fully differentiable network with  $R$  recurrences, which we named Adaptive Path Integral Autoencoder (APIAE). Note that the inference, reconstruction, and gradient backpropagation of APIAE can operate independently for each of  $L$  samples. Consequently, the computational cost grows linearly with the number of samples,  $L$ , and the number of adaptations,  $R$ . As implemented in IWAE [Burda et al., 2016], we replicated each observation data  $L$  times and the whole operations were parallelized with GPU. We implemented APIAE with Tensorflow [Abadi et al., 2016]; the pseudo code and algorithmic details of APIAE are given in the Appendix C and the implementation code will be made available online.

## 4 High-dimensional Motion Planning with Learned Latent Model

The learned latent dynamical model can be exploited to generate a high-dimensional motion plan. High-dimensional motion planning is a challenging problem because of the curse of dimensionality: The size of the configuration space exponentially increases with the number of dimensions. However, it might be a reasonable assumption that configurations that a planning algorithm really needs to consider form some sort of low-dimensional manifold in the configuration space [Vernaza and Lee, 2012] and the learned generative model provides stochastic dynamics in that manifold. Once this low-dimensional representation is obtained, any motion planning algorithm can solve high-dimensional planning problem very efficiently, because its search space is greatly restricted.

More formally, suppose that the initial configuration,  $\mathbf{x}_1$ , and corresponding latent state  $\mathbf{z}(0)$  are given and the cost function,  $C_k(\mathbf{x}_k)$ , encodes given task specifications of a planning problem, e.g.,

desirability/undesirability of certain configurations, a penalty for obstacle collision, etc. Then, the planning problem can be converted into the problem of finding the optimal trajectory distribution,  $q_{\mathbf{u}}$ , that minimizes the following objective function:

$$J(q_{\mathbf{u}}) = \mathbb{E}_{\mathbf{x}_{1:K} \sim p_{\theta}(\cdot | \mathbf{z}_{[0,T]}), \mathbf{z}_{[0,T]} \sim q_{\mathbf{u}}(\cdot)} \left[ \sum_{k=1}^K C_k(\mathbf{x}_k) + D_{KL}(q_{\mathbf{u}}(\mathbf{z}_{[0,T]}) || p_{\theta}(\mathbf{z}_{[0,T]})) \right]. \quad (19)$$

That is, we want to find parameters,  $\mathbf{u}$ , of the trajectory distribution which not only likely generates sample configuration sequences achieving the lower planning cost but also does not deviate a lot from the (learned) prior,  $p_{\theta}(\mathbf{z}_{[0,T]})$ . The solution can be found using the aforementioned adaptive path integral control method, where its state cost function is set as:  $V(\mathbf{z}_{[0,T]}) \equiv \mathbb{E}_{p_{\theta}(\mathbf{x}_{1:K} | \mathbf{z}_{[0,T]})} \left[ \sum_{k=1}^K C_k(\mathbf{x}_k) \right]$  and the initial state distribution is not updated in the adaptation process. After the adaptations with this state cost function, the resulting plan can simply be sampled from the generative model, e.g.,  $\mathbf{x}_{1:K} \sim p_{\theta}(\cdot | \mu_{[0,T]})$ . Note that the time interval  $t_k - t_{k-1}$  and the trajectory length  $K$  can differ in the training and planning phases because continuous-time dynamics is dealt with.

## 5 Related Work

To address the complexity raised from temporal structures of data, several approaches that build a sophisticated approximate inference model have been proposed. For example, Karl et al. [2017] used the locally linear latent dynamics by introducing transition parameters, where an inference model infers transition parameters rather than latent states from the local transition. Johnson et al. [2016] combined a structured graphical model in latent space with a deep generative network, where an inference network produces local evidence potentials for the message passing algorithms. Fraccaro et al. [2017] constructed two layers of latent models, where linear-Gaussian dynamical systems governed two latent layers and the observation at each time step was related to the middle layer independently; the inference model in this framework consists of independent VAE’s inference networks at each time-step and the Kalman smoothing algorithm along the time axis. Finally, deep Kalman smoother (DKS) in [Krishnan et al., 2017] parameterized the dynamical system by a deep neural network and built an inference network as it has the same structure with the factorized posterior distribution. The idea of MCOs was also used in the temporal setting. Maddison et al. [2017], Le et al. [2018], Naesseth et al. [2018] adapted the particle filter (PF) algorithm as their inference models and utilized a PF’s estimator of the marginal likelihood as an objective function of training, which Maddison et al. [2017] named the filtering variational objectives (FIVOs).

These approaches can be viewed as attempts to reduce the approximation gap; by building the inference model in sophisticated ways that exploit underlying structure of data, the resulting variational family could flexibly approximate the posterior distribution. To overcome the amortization gap caused by inference networks, the semi-amortized method utilizes an iterative refinement procedure for improving variational distribution. Let  $q_{\phi}$  and  $q^*$  be the variational distributions from the inference network and from the refinement procedure, respectively. Hjelm et al. [2016] adopted adaptive importance sampling to refine the variational parameters, and the generative and inference networks are trained separately with  $\nabla_{\theta} \mathcal{L}(q^*, \theta; \mathbf{x})$  and  $\nabla_{\phi} D_{KL}(q^* || q_{\phi})$ , respectively. Krishnan et al. [2018] used stochastic variational inference as a refinement procedure, and the generative and inference networks are also trained separately with  $\nabla_{\theta} \mathcal{L}(q^*, \theta; \mathbf{x})$  and  $\nabla_{\phi} \mathcal{L}(q_{\phi}, \theta; \mathbf{x})$ , respectively. Kim et al. [2018] also used stochastic variational inference but proposed the *end-to-end* training by allowing the learning signals to be backpropagated into the refinement procedure, and showed this end-to-end training outperformed the separate training.

This work presents a semi-amortized variational inference method for temporal data. In summary, we parameterize the variational distribution by control input and transformed the approximate inference into the SOC problem. Our method utilizes the structured inference network based on the principle of optimality which has a similar structure to the inference network of DKS [Krishnan et al., 2017]. The adaptive path-integral control method, which can be viewed as adaptive importance sampling in trajectory space [Kappen and Ruiz, 2016], is then adopted as a refinement procedure. Ruiz and Kappen [2017] also used the adaptive path integral approach to solve smoothing problems and showed the path integral-based smoothing method could outperform the PF-based smoothing algorithms. Finally, by observing all procedures of the path integral smoothing are differentiable, the inference and generative networks are trained in the end-to-end manner. Note that APIAE is not the first algorithm

that implements an optimal planning/control algorithm into a fully-differentiable network. In Tamar et al. [2016], Okada et al. [2017], Karkus et al. [2017], similar iterative refinement procedures were built as differentiable networks to learn solutions of control problems in an end-to-end manner; the fact that iterative methods were generally used to solve control problems could be a rationale for utilizing refinement to approximate inference.

There is a *non-probabilistic* branch of representation learning of dynamical systems, e.g., [Watter et al., 2015, Banijamali et al., 2018, Jonschkowski and Brock, 2015, Lesort et al., 2018]. They basically stack two consecutive observations to contain the temporal information and learn the dynamical model based on a carefully designed loss function considering the stacked data as one observation. As shown in Appendix D, however, when the observations are highly-noisy (or even worse, when the system is unobservable with the stacked data), stacking a small number of observations prohibits the training data from containing enough temporal information for learning rich generative models.

Meanwhile, there have been some recent works to utilize a low-dimensional latent model for motion planning. Chen et al. [2016] exploited the idea of VAEs to embed dynamic movement primitives into the latent space. In [Ha et al., 2018], Gaussian process dynamical model [Wang et al., 2008] served as a latent dynamical model and was utilized for planning in a similar way with this work. Finally, though the dynamics were not considered, Ichter et al. [2018], Zhang et al. [2018] used the conditional VAEs to learn a non-uniform sampling methodology of a sampling-based motion planning algorithm.

## 6 Experiments

In our experiments, we would like to show that the proposed method is complementary technique to the existing methods; the APIAE can play a role in constructing more expressive posterior distribution by refining the variational distribution from the existing approximate inference methods. To support our statement, we built APIAEs upon the FIVO and IWAE frameworks and compared with the model without adaptation procedures.

We set our APIAE parameters as  $L=8$ ,  $R=4$ , and  $K=10$  during experiments. Quantitative studies about the effect of varying these parameters are discussed in the appendix. Feedback gain is only used for the planning, since matrix inversion in (16) requires Cholesky decomposition which is often numerically unstable during the training. We would refer the readers to the Appendix D and the supplementary video at <https://youtu.be/NLM0GQ0o4jM> for more experimental details and results.

### 6.1 Dynamic Pendulum

The first experiment addresses the system identification and planning of inverted pendulum with the raw images. The pendulum dynamics is represented by the second order differential equation for angle of the pendulum,  $\psi$ , as  $\ddot{\psi} = -9.8 \sin(\psi) - \dot{\psi}$ . We simulated the pendulum dynamics by injecting the disturbance from random initial states and then made sequences of  $16 \times 16$  sized images corresponding to the pendulum state with the time interval,  $\delta t = 0.1$ . This set of sequence images was the training data of APIAE, i.e.,  $\mathbf{x}_k$  lied in 256-dimensional observation space. 3000 and 500 data are used for training and test, respectively.

Fig. 1(a) shows the constructed 2-D latent space; each point represents the posterior mean of the observation data and it is shown that the angle and the angular velocity are well-encoded into 2-D space. As shown in Fig. 1(b), the learned dynamical model was able to successfully reconstruct the noisy observations, predict and plan the future images. For the planning, the cost functions were set to penalize the difference between the last image of the generated sequence and the target image in Fig. 1(c).

### 6.2 Human Motion Capture Data

The second experiment addresses a motion planning of a humanoid robot with 62-dimensional configuration space. We utilized human motion capture data from the Carnegie Mellon University motion capture (CMU mocap) database for the learning; the training data was a set of (short) locomotions, e.g., for standing, walking, and turning. The 62-dimensional configurations consist of angles of all joints, roll and pitch angles, vertical position of the root, yaw rate of the root,

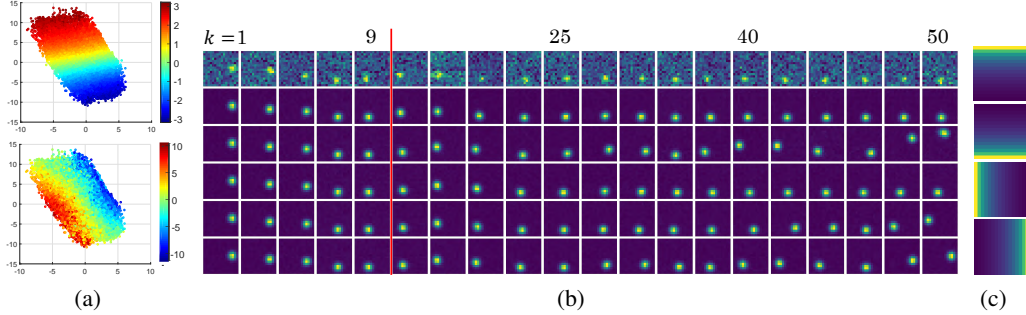


Figure 1: Pendulum results. (a) The inferred latent states colored by angles (top) and angular velocities (bottom) of the ground truth. (b) Resulting image sequences. From the top: images of ground truth, prediction, and four planning results for swing-up, -down, -left, and -right, respectively. Except the first row, the images before the red line ( $k \leq 10$ ) are reconstructed one. (c) The target images for each task:  $C_K = \|\mathbf{x}_{target} - \mathbf{x}_K\|^2$ .

and horizontal velocity of the root. The global (horizontal) position and heading orientation are not encoded in the generative model (only velocities are encoded), but they can be recovered by integration when the trajectory is given. The original data were written at 120 Hz, and we down-sampled them to 20 Hz and cut them every 10 time steps, i.e.,  $\delta t = 0.05$ ,  $K = 10$ . 1043 and 173 data are used for training and test, respectively. We utilized the DeepMind Control Suite [Tassa et al., 2018] for parsing the data and visualizing the results.

Figs. 2(a-c) illustrate the posterior mean states of the training data colored by some physical quantities of the ground truth data; we can observe that (a) locomotion is basically embedded along the surface of the cylinder, while (b) they were arranged in the order of the yaw rates along the major axis of the cylinder and (c) motions with lower forward velocities were embedded into smaller radius cycles. Also, Fig. 2(d) shows that APIAE successfully reconstructed the data. Compared to the pendulum example, where the Wiener process in latent dynamics models disturbance into the system and the prediction can be made simply by ignoring the disturbance, the framework in this example uses the Wiener process to model the uncertainty in human’s decision, similar to the modeling of the bounded rationality [Genewein et al., 2015] or the maximum entropy IRL [Ziebart et al., 2008]; as shown in Fig. 2(e), from the very same initial pose, the framework predicts multiple future configurations for, e.g., going straight, turning left or right (the ratio between motions eventually matches that of the training dataset) and these predictions play essential roles in the planning. We then formulated planning problems, where the cost function penalized collision with any obstacle, large yaw rate, and distance from the goal. Figs. 2(f-g) show that the proposed method successfully generated the natural and collision-free motion toward the goal.

### 6.3 Quantitative Results

It is easily thought that powerful inference methods via resampling or refinements make the bound tighter, but achieving a tighter bound during learning does not directly imply a better model learning [Rainforth et al., 2018]. To investigate this, we have compared the lower bound, the reconstruction and prediction abilities of the models learned by the proposed and baseline algorithms. The results are reported in Table 1 (higher is better).<sup>2</sup> Interestingly, we can observe that learning with both the resampling and path-integral refinements resulted in the best reconstruction ability as well as the tightest bound, but the best prediction was achieved by the model learned only with the refinements. It implies that while powerful inference can lead to a tighter bound and a good reconstruction, a bias in the gradients can prevent the resulting model from being accurate (note that the gradient components from the resampling are generally ignored because it causes high variance of the gradient estimator). In the planning side, the prediction power is more crucial because the (learned) generative model needs to sample meaningful and diverse configuration sequences. We conclude that the resampling procedure would be better to utilize only for planning, not for learning, and this also would be the

<sup>2</sup>Mocap prediction is omitted, because it is hard to define a proper measure for this prediction.



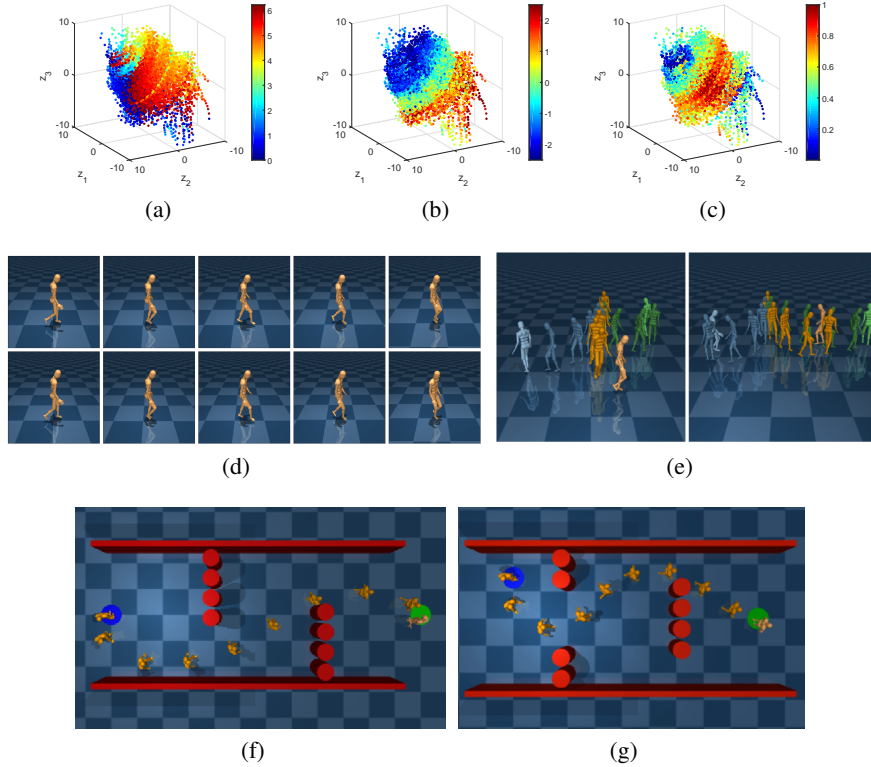


Figure 2: Mocap results. The learned latent space colored by (a) the gait phase, (b) yaw rate, and (c) forward velocity of the ground truth. We set the phase to 0 when the left feet touch the ground and to  $\pi$  when the right feet touch the ground. (d) Reconstruction. (e) Prediction results from the same initial poses. (f-g) Locomotion planning results. The start and goal regions are represented as blue and green circles, respectively.

same in other application domains like 3-D human motion tracking, where the prediction ability is more important.

Table 1: Comparison of the lower bound, reconstruction, and prediction. Each model was trained with (i) APIAE with resampling (+r), (ii) APIAE without resampling, (iii) FIVO, and (iv) IWAE. The lower bounds are obtained for the training datasets and the reconstruction and prediction results are made for the test datasets; the amounts of the test datasets were around 1/6 of the training datasets.

|         | Pendulum ( $\times 10^6$ ) |                |               | Mocap ( $\times 10^5$ ) |                |
|---------|----------------------------|----------------|---------------|-------------------------|----------------|
|         | Lower-bound                | Reconstruction | Prediction    | Lower-bound             | Reconstruction |
| APIAE+r | <b>-9.866</b>              | <b>-1.647</b>  | -1.985        | <b>-6.665</b>           | <b>-1.158</b>  |
| APIAE   | -9.927                     | -1.653         | <b>-1.845</b> | -6.680                  | -1.171         |
| FIVO    | -9.890                     | -1.650         | -1.978        | -6.687                  | -1.167         |
| IWAE    | -9.974                     | -1.665         | -1.860        | -6.683                  | -1.174         |

## 7 Conclusion

In this paper a semi-amortized variational inference method for temporal data was proposed. We parameterized the variational distribution by control input and transformed the approximate inference into SOC problem. The proposed framework utilized the structured inference network based on the principle of optimality and adopted the adaptive path-integral control method as a refinement procedure. The experiments showed that the refinement procedure helped the learning algorithm

achieve tighter lower bound. Also, it is shown that the valid dynamical model can be identified from sequential raw data and utilized to plan the future configurations.

## References

- Martín Abadi, Paul Barham, Jianmin Chen, Zhifeng Chen, Andy Davis, Jeffrey Dean, Matthieu Devin, Sanjay Ghemawat, Geoffrey Irving, Michael Isard, et al. Tensorflow: A system for large-scale machine learning. In *OSDI*, volume 16, pages 265–283, 2016.
- Ershad Banijamali, Rui Shu, Mohammad Ghavamzadeh, Hung Bui, and Ali Ghodsi. Robust locally-linear controllable embedding. *International Conference on Artificial Intelligence and Statistics (AISTATS)*, 2018.
- Richard Bellman. *Dynamic programming*. Courier Corporation, 2013.
- Yuri Burda, Roger Grosse, and Ruslan Salakhutdinov. Importance weighted autoencoders. *International Conference on Learning Representations (ICLR)*, 2016.
- Nutan Chen, Maximilian Karl, and Patrick van der Smagt. Dynamic movement primitives in latent space of time-dependent variational autoencoders. In *International Conference on Humanoid Robots (Humanoids)*, pages 629–636. IEEE, 2016.
- Chris Cremer, Quaid Morris, and David Duvenaud. Reinterpreting importance-weighted autoencoders. *ICLR Workshop*, 2017.
- Chris Cremer, Xuechen Li, and David Duvenaud. Inference suboptimality in variational autoencoders. *arXiv preprint arXiv:1801.03558*, 2018.
- Marco Fraccaro, Simon Kamronn, Ulrich Paquet, and Ole Winther. A disentangled recognition and nonlinear dynamics model for unsupervised learning. In *Advances in Neural Information Processing Systems (NIPS)*, pages 3604–3613, 2017.
- Crispin W Gardiner et al. *Handbook of stochastic methods*, volume 4. Springer Berlin, 1985.
- Tim Genewein, Felix Leibfried, Jordi Grau-Moya, and Daniel Alexander Braun. Bounded rationality, abstraction, and hierarchical decision-making: An information-theoretic optimality principle. *Frontiers in Robotics and AI*, 2:27, 2015.
- Jung-Su Ha, Hyeok-Joo Chae, and Han-Lim Choi. Approximate inference-based motion planning by learning and exploiting low-dimensional latent variable models. In *Robotics and Automation Letters (RA-L/ROS'18)*. IEEE, 2018.
- Devon Hjelm, Ruslan R Salakhutdinov, Kyunghyun Cho, Nebojsa Jojic, Vince Calhoun, and Junyoung Chung. Iterative refinement of the approximate posterior for directed belief networks. In *Advances in Neural Information Processing Systems (NIPS)*, pages 4691–4699, 2016.
- Brian Ichter, James Harrison, and Marco Pavone. Learning sampling distributions for robot motion planning. *International Conference on Robotics and Automation (ICRA)*, 2018.
- Matthew Johnson, David K Duvenaud, Alex Wiltschko, Ryan P Adams, and Sandeep R Datta. Composing graphical models with neural networks for structured representations and fast inference. In *Advances in neural information processing systems (NIPS)*, pages 2946–2954, 2016.
- Rico Jonschkowski and Oliver Brock. Learning state representations with robotic priors. *Autonomous Robots*, 39(3):407–428, 2015.
- Hilbert Johan Kappen and Hans Christian Ruiz. Adaptive importance sampling for control and inference. *Journal of Statistical Physics*, 162(5):1244–1266, 2016.
- Peter Karkus, David Hsu, and Wee Sun Lee. Qmdp-net: Deep learning for planning under partial observability. In *Advances in Neural Information Processing Systems (NIPS)*, pages 4697–4707, 2017.

- Maximilian Karl, Maximilian Soelch, Justin Bayer, and Patrick van der Smagt. Deep variational bayes filters: Unsupervised learning of state space models from raw data. *International Conference on Learning Representations (ICLR)*, 2017.
- Yoon Kim, Sam Wiseman, Andrew C Miller, David Sontag, and Alexander M Rush. Semi-amortized variational autoencoders. *arXiv preprint arXiv:1802.02550*, 2018.
- Diederik P Kingma and Max Welling. Auto-encoding variational bayes. *International Conference on Learning Representations (ICLR)*, 2014.
- Rahul G Krishnan, Uri Shalit, and David Sontag. Structured inference networks for nonlinear state space models. In *AAAI*, pages 2101–2109, 2017.
- Rahul G Krishnan, Dawen Liang, and Matthew Hoffman. On the challenges of learning with inference networks on sparse, high-dimensional data. *International Conference on Artificial Intelligence and Statistics (AISTATS)*, 2018.
- Tuan Anh Le, Maximilian Igl, Tom Jin, Tom Rainforth, and Frank Wood. Auto-encoding sequential monte carlo. *International Conference on Learning Representations (ICLR)*, 2018.
- Timothée Lesort, Natalia Díaz-Rodríguez, Jean-François Goudou, and David Filliat. State representation learning for control: An overview. *arXiv preprint arXiv:1802.04181*, 2018.
- Chris J Maddison, Dieterich Lawson, George Tucker, Nicolas Heess, Mohammad Norouzi, Andriy Mnih, Arnaud Doucet, and Yee Whye Teh. Filtering variational objectives. In *Advances in neural information processing systems (NIPS)*, 2017.
- Andriy Mnih and Danilo Rezende. Variational inference for monte carlo objectives. In *International Conference on Machine Learning (ICML)*, pages 2188–2196, 2016.
- Christian A Naesseth, Scott W Linderman, Rajesh Ranganath, and David M Blei. Variational sequential monte carlo. In *International Conference on Artificial Intelligence and Statistics (AISTATS)*, 2018.
- Masashi Okada, Luca Rigazio, and Takenobu Aoshima. Path integral networks: End-to-end differentiable optimal control. *arXiv preprint arXiv:1706.09597*, 2017.
- Tom Rainforth, Adam R Kosiorek, Tuan Anh Le, Chris J Maddison, Maximilian Igl, Frank Wood, and Yee Whye Teh. Tighter variational bounds are not necessarily better. In *International Conference on Machine Learning (ICML)*, 2018.
- Danilo Jimenez Rezende, Shakir Mohamed, and Daan Wierstra. Stochastic backpropagation and approximate inference in deep generative models. In *International Conference on Machine Learning (ICML)*, pages 1278–1286, 2014.
- Hans-Christian Ruiz and Hilbert J Kappen. Particle smoothing for hidden diffusion processes: Adaptive path integral smoother. *IEEE Transactions on Signal Processing*, 65(12):3191–3203, 2017.
- Aviv Tamar, Yi Wu, Garrett Thomas, Sergey Levine, and Pieter Abbeel. Value iteration networks. In *Advances in Neural Information Processing Systems (NIPS)*, pages 2154–2162, 2016.
- Yuval Tassa, Yotam Doron, Alistair Muldal, Tom Erez, Yazhe Li, Diego de Las Casas, David Budden, Abbas Abdolmaleki, Josh Merel, Andrew Lefrancq, et al. DeepMind Control Suite. *arXiv preprint arXiv:1801.00690*, 2018.
- Sep Thijssen and HJ Kappen. Path integral control and state-dependent feedback. *Physical Review E*, 91(3):032104, 2015.
- Emanuel Todorov. General duality between optimal control and estimation. In *IEEE Conference on Decision and Control*, pages 4286–4292. IEEE, 2008.
- Emanuel Todorov. Efficient computation of optimal actions. *Proceedings of the national academy of sciences*, 106(28):11478–11483, 2009.

- Paul Vernaza and Daniel D Lee. Learning and exploiting low-dimensional structure for efficient holonomic motion planning in high-dimensional spaces. *The International Journal of Robotics Research*, 31(14):1739–1760, 2012.
- Jack M Wang, David J Fleet, and Aaron Hertzmann. Gaussian process dynamical models for human motion. *IEEE transactions on pattern analysis and machine intelligence*, 30(2):283–298, 2008.
- Manuel Watter, Jost Springenberg, Joschka Boedecker, and Martin Riedmiller. Embed to control: A locally linear latent dynamics model for control from raw images. In *Advances in neural information processing systems (NIPS)*, pages 2746–2754, 2015.
- Clark Zhang, Jinwook Huh, and Daniel D Lee. Learning implicit sampling distributions for motion planning. *arXiv preprint arXiv:1806.01968*, 2018.
- Brian D Ziebart, Andrew L Maas, J Andrew Bagnell, and Anind K Dey. Maximum entropy inverse reinforcement learning. In *AAAI*, volume 8, pages 1433–1438. Chicago, IL, USA, 2008.

## A Objective Function of Linearly-Solvable Optimal Control

Suppose that an objective function of a SOC problem is given as:

$$J = \mathbb{E}_{q_{\mathbf{u}}} \left[ \int_0^T V(\mathbf{z}(t)) + \frac{1}{2} \|\mathbf{u}(t)\|^2 dt \right] + D_{KL}(q_0(\mathbf{z}(0)) \| p_0(\mathbf{z}(0))), \quad (20)$$

where  $q_{\mathbf{u}}$  is the probability measures induced by the controlled trajectories from (9). The first and second terms in the integral encodes a state cost and regulates control input effort, respectively, and the last KL term penalizes the initial state deviation. The objective of the SOC problem is to find the optimal control sequence  $\mathbf{u}^*(t)$  as well as the initial state distribution  $q_0$ , with which the trajectory distribution of (9) minimizes the objective function (20).

The following theorem implies that the control penalty term in (20) can be interpreted as the KL-divergence between distributions of controlled and uncontrolled trajectories.

**Theorem 1 (Girsanov's Theorem (modified from Gardiner et al. [1985]))** *Suppose  $p$  and  $q_{\mathbf{u}}$  are the probability measures induced by the trajectories of (3) and (9), respectively. Then, the Radon-Nikodym derivative of  $q_{\mathbf{u}}$  with respect to  $p$  is given by*

$$\frac{dp(\mathbf{z}_{[0,T]})}{dq_{\mathbf{u}}(\mathbf{z}_{[0,T]})} = \frac{p_0(\mathbf{z}(0))}{q_0(\mathbf{z}(0))} \exp \left( -\frac{1}{2} \int_0^T \|\mathbf{u}(t)\|^2 dt - \int_0^T \mathbf{u}(t)^T d\mathbf{w}(t) \right), \quad (21)$$

where  $\mathbf{w}(t)$  is a Wiener process for simulating  $q_{\mathbf{u}}$ .

With Girsanov's theorem, the objective function (20) is rewritten in the form of the KL-divergence:

$$\begin{aligned} J &= \mathbb{E}_{q_{\mathbf{u}}} \left[ \int_0^T V(\mathbf{z}(t)) + \frac{1}{2} \|\mathbf{u}(t)\|^2 dt \right] + D_{KL}(q_0(\mathbf{z}(0)) \| p_0(\mathbf{z}(0))) \\ &= \mathbb{E}_{q_{\mathbf{u}}} \left[ \int_0^T V(\mathbf{z}(t)) dt + \log \frac{dq_{\mathbf{u}}(\mathbf{z}_{[0,T]})}{dp(\mathbf{z}_{[0,T]})} - \log \frac{q_0(\mathbf{z}(0))}{p_0(\mathbf{z}(0))} \right] + D_{KL}(q_0(\mathbf{z}(0)) \| p_0(\mathbf{z}(0))) \\ &= \mathbb{E}_{q_{\mathbf{u}}} \left[ \log \frac{dq_{\mathbf{u}}(\mathbf{z}_{[0,T]})}{dp(\mathbf{z}_{[0,T]}) \exp(-V(\mathbf{z}_{[0,T]})/\xi)} - \log \xi \right] \\ &= D_{KL}(q_{\mathbf{u}}(\mathbf{z}_{[0,T]}) \| p^*(\mathbf{z}_{[0,T]})) - \log \xi, \end{aligned} \quad (22)$$

where  $V(\mathbf{z}_{[0,T]}) \equiv \int_0^T V(\mathbf{z}(t)) dt$  is a trajectory state cost and  $\xi \equiv \int \exp(-V(\mathbf{z}_{[0,T]})) dp(\mathbf{z}_{[0,T]})$  is a normalization constant. Note that the second term in the exponent of (21) disappears when taking expectation w.r.t.  $q_{\mathbf{u}}$ , i.e.  $\mathbb{E}_{q_{\mathbf{u}}}[\int_0^T \mathbf{u}(t)^T d\mathbf{w}(t)] = 0$ , because  $\mathbf{w}(t)$  is a Wiener process for simulating  $q_{\mathbf{u}}$ . Because  $\xi$  is not a function of  $\mathbf{u}$ ,  $p^*(\mathbf{z}_{[0,T]})$  can be interpreted as the optimally-controlled trajectory distribution that minimizes the objective function,  $J$ :

$$dp^*(\mathbf{z}_{[0,T]}) = \frac{\exp(-V(\mathbf{z}_{[0,T]})) dp(\mathbf{z}_{[0,T]})}{\int \exp(-V(\mathbf{z}_{[0,T]})) dp(\mathbf{z}_{[0,T]})} \quad (23)$$

$$\propto dp(\mathbf{z}_{[0,T]}) \exp(-V(\mathbf{z}_{[0,T]})). \quad (24)$$

This expression yields the method to sample the optimally-controlled trajectories: We first sample a set of trajectories according to the passive dynamics, i.e.,  $\mathbf{z}_{[0,T]}^l \sim p(\cdot)$ , which can be interpreted as the proposal distribution, and assign their importance weights as  $\tilde{w}^l \propto \exp(-V(\mathbf{z}_{[0,T]}^l))$ ,  $\forall l$  and  $\sum_l \tilde{w}^l = 1$ .

The proposal distribution can be changed into the controlled trajectory distribution so as to increase the sample efficiency. By applying the Girsanov's theorem again, the optimal trajectory distribution is expressed as:

$$dp^*(\mathbf{z}_{[0,T]}) \propto dq_{\mathbf{u}}(\mathbf{z}_{[0,T]}) \exp(-S_{\mathbf{u}}(\mathbf{z}_{[0,T]})), \quad (25)$$

where

$$S_{\mathbf{u}}(\mathbf{z}_{[0,T]}) = V(\mathbf{z}_{[0,T]}) + \frac{1}{2} \int_0^T \|\mathbf{u}(t)\|^2 dt + \int_0^T \mathbf{u}(t)^T d\mathbf{w}(t). \quad (26)$$

This yields that the optimal trajectory distribution can be obtained by sampling a set of trajectories according to the controlled dynamics with  $\mathbf{u}(t)$ , i.e.,  $\mathbf{z}_{[0,T]}^l \sim q_{\mathbf{u}}(\cdot)$ , and assigning their importance weights as  $\tilde{w}^l \propto \exp(-S_{\mathbf{u}}(\mathbf{z}_{[0,T]}^l))$ ,  $\forall l$  and  $\sum_l \tilde{w}^l = 1$ . It is known that, as the control input  $\mathbf{u}(\cdot)$  gets closer to the true optimal control input  $\mathbf{u}^*(\cdot)$ , the variance of importance weights decreases and it reduces to 0 when  $\mathbf{u}(t) = \mathbf{u}^*(t, \mathbf{z}(t))$  [Thijssen and Kappen, 2015].

## B Derivation of Path Integral Adaptation

From the trajectories sampled with  $q_{\mathbf{u}}(\cdot)$ , the path integral control provides how to compute the optimal control  $\mathbf{u}^*(t)$  based on the following theorem.

**Theorem 2 (Main Theorem [Thijssen and Kappen, 2015])** *Let  $f : \mathbb{R} \times \mathbb{R}^{d_z} \rightarrow \mathbb{R}$ , and consider the process  $f(t) = f(t, \mathbf{z}(t))$  with  $\mathbf{z}_{[0,T]} \sim q_{\mathbf{u}}(\cdot)$ . Then,*

$$\langle (\mathbf{u}^* - \mathbf{u})f \rangle (t) = \lim_{\tau \rightarrow t} \left\langle \frac{\int_t^\tau f(s) d\mathbf{w}(s)}{\tau - t} \right\rangle, \quad (27)$$

where  $\langle Y(t) \rangle \equiv \mathbb{E}_{q_{\mathbf{u}}}[\tilde{w}_{\mathbf{u}} Y(t)]$ ,  $\tilde{w}_{\mathbf{u}} = \frac{\exp(-S_{\mathbf{u}}(\mathbf{z}_{[0,T]}))}{\mathbb{E}_{q_{\mathbf{u}}}[\exp(-S_{\mathbf{u}}(\mathbf{z}_{[0,T]}))]}$  for any process  $Y(t)$ .

Suppose the current control policy is parameterized with  $n_b$  basis functions  $\bar{h}(t, \mathbf{z}) : \mathbb{R} \times \mathbb{R}^{d_z} \rightarrow \mathbb{R}^{n_b}$  as:

$$\bar{\mathbf{u}}(t, \mathbf{z}(t)) = \bar{\mathbf{A}}(t) \bar{h}(t, \mathbf{z}(t)), \quad (28)$$

where  $\bar{\mathbf{A}}(t) : \mathbb{R} \rightarrow \mathbb{R}^{d_u \times n_b}$  is the control policy parameter and let the optimal parameterized control policy be  $\mathbf{u}^* = \mathbf{A}^*(t) h(t, \mathbf{z}(t))$ . Then, Theorem 2 can be rewritten as:

$$\mathbf{A}^*(t) \langle h \otimes h \rangle (t) = \bar{\mathbf{A}}(t) \langle \bar{h} \otimes h \rangle (t) + \lim_{\tau \rightarrow t} \left\langle \frac{\int_t^\tau d\mathbf{w}(s) \otimes h(s)}{\tau - t} \right\rangle. \quad (29)$$

Because we can utilize only a finite number of samples to approximate the optimal trajectory distribution, it is more reasonable to update the control policy parameter with some small adaptation rate, than to estimate it at once. Similar to Ruiz and Kappen [2017], we use a standardized linear feedback controller w.r.t. the target distribution, i.e.,

$$h(t, \mathbf{z}(t)) \equiv \left[ \mathbf{1}; \Sigma^{-1/2}(t)(\mathbf{z}(t) - \mu(t)) \right], \quad (30)$$

where  $\mu(t) = \langle \mathbf{z}(t) \rangle$  and  $\Sigma(t) = \langle (\mathbf{z}(t) - \mu(t))(\mathbf{z}(t) - \mu(t))^T \rangle$  are the mean and covariance of the state w.r.t. the optimal trajectory distribution estimated at the previous iteration. Then, the control input has a form as:

$$\mathbf{u}(t) = \mathbf{u}^{ff}(t) + \mathbf{K}(t) \Sigma^{-1/2}(t)(\mathbf{z}(t) - \mu(t)), \quad (31)$$

where the parameter,  $\mathbf{A}(t) = [\mathbf{u}^{ff}(t), \mathbf{K}(t)]$ , represents feedforward control signal and feedback gain.

Suppose we have a set of trajectories and their weights obtained by the parameterized policy,  $\bar{\mathbf{u}}(t) = \bar{\mathbf{A}}(t) \bar{h}(t, \mathbf{z}(t))$ . Then, based on (29), the control policy parameters can be updated as follows:

$$\mathbf{u}^{ff}(t) dt = \bar{\mathbf{u}}^{ff}(t) dt + \bar{\mathbf{K}}(t) \bar{\Sigma}^{-1/2}(t)(\mu(t) - \bar{\mu}(t)) dt + \eta \langle d\mathbf{w}(t) \rangle, \quad (32)$$

$$\mathbf{K}(t) dt = \bar{\mathbf{K}}(t) \bar{\Sigma}^{-1/2}(t) \Sigma^{1/2}(t) dt + \eta \left\langle d\mathbf{w}(t) \left( \Sigma^{-1/2}(t)(\mathbf{z}(t) - \mu(t)) \right)^T \right\rangle, \quad (33)$$

where  $\eta$  is an adaptation rate<sup>3</sup>. Note that the adaptation of two terms can be done independently, because  $\langle h \otimes h \rangle (t) = I$ . Beside the control policy adaptation, the initial state distribution,  $p_0$ , can be updated as well:

$$\hat{\mu}_0 = \langle \mathbf{z}(0) \rangle, \quad \hat{\Sigma}_0 = \langle (\mathbf{z}(0) - \hat{\mu}_0)(\mathbf{z}(0) - \hat{\mu}_0)^T \rangle, \quad (34)$$

where the updated trajectory distribution starts from  $q_0(\cdot) = \mathcal{N}(\cdot; \hat{\mu}_0, \hat{\Sigma}_0)$ . The whole procedures are summarized in Algorithm 1.

---

**Algorithm 1** Path Integral Adaptation

---

**Input:** Dynamics,  $\mathbf{f}(\mathbf{z})$ ,  $\sigma(\mathbf{z})$ , initial state distribution,  $\hat{\mu}_0, \hat{\Sigma}_0$ , and control policy parameters,  $\mathbf{A}_{[0,T]}$ .

```
1: for  $r \in \{1, \dots, R\}$  do
2:    $\{S_{\mathbf{u}}, \hat{w}, \mathbf{z}_{[0,T]}, \mathbf{w}_{[0,T]}\}^{1:L} \leftarrow \text{SIMULATE}(\hat{\mu}_0, \hat{\Sigma}_0, \mathbf{A}_{[0,T]})$ 
3:    $\hat{\mu}_0, \hat{\Sigma}_0, \mathbf{A}_{[0,T]} \leftarrow \text{IMPROVE}(\{\hat{w}, \mathbf{z}_{[0,T]}, \mathbf{w}_{[0,T]}\}^{1:L}, \mathbf{A}_{[0,T]})$   $\triangleright$  using (15)-(16) and (17)
4: end for
5:  $\{S_{\mathbf{u}}, \mathbf{z}_{[0,T]}, \mathbf{w}_{[0,T]}\}^{1:L} \leftarrow \text{SIMULATE}(\hat{\mu}_0, \hat{\Sigma}_0, \mathbf{A}_{[0,T]})$ 
6: return  $\{\mathbf{z}_{[0,T]}, S_{\mathbf{u}}, \hat{w}\}^{1:L}$ 

1: function  $\text{SIMULATE}(\hat{\mu}_0, \hat{\Sigma}_0, \mathbf{A}_{[0,T]})$   $\triangleright$  Stochastic simulation via Euler method
2:    $\mathbf{z}_1^{1:L} \leftarrow \text{SAMPLENORMAL}(\hat{\mu}_0, \hat{\Sigma}_0)$ 
3:   for  $k \in \{1, \dots, K-1\}$  do
4:     for  $l \in \{1, \dots, L\}$  do
5:        $d\mathbf{w}_{k-1}^{(l)} \leftarrow \text{SAMPLENORMAL}(0, \sqrt{\delta t}I)$ 
6:        $\mathbf{z}_k^{(l)} \leftarrow \mathbf{z}_{k-1}^{(l)} + \mathbf{f}(\mathbf{z}_{k-1}^{(l)})\delta t + \sigma(\mathbf{z}_{k-1}^{(l)})(\mathbf{u}_{k-1}^{(l)}\delta t + d\mathbf{w}_{k-1}^{(l)})$   $\triangleright \mathbf{u}_{k-1}^{(l)}$  from (28).
7:        $S_{\mathbf{u}}^{(l)} \leftarrow S_{\mathbf{u}}^{(l)} + V(\mathbf{z}_k^{(l)})\delta t + \frac{1}{2}\|\mathbf{u}_{k-1}^{(l)}\|^2\delta t + (\mathbf{u}_{k-1}^{(l)})^T d\mathbf{w}_{k-1}^{(l)}$ 
8:        $\hat{w}^{1:L} \leftarrow \exp(-S_{\mathbf{u}}^{1:L}) / \sum_l \exp(-S_{\mathbf{u}}^l)$ 
9:       (Optional) Resample if effective sample size of  $\hat{w}^{1:L}$  is smaller than threshold
10:    end for
11:  end for
12:  return  $\{S_{\mathbf{u}}, \hat{w}, \mathbf{z}_{[0,T]}, \mathbf{w}_{[0,T]}\}^{1:L}$ 
13: end function
```

---

---

**Algorithm 2** Structured inference network  $h_\phi$  (Figure 3)

---

**Input:** A observation sequence,  $\mathbf{x}_{1:K}$ .

```
1:  $\mathbf{h}_K \leftarrow h_{\phi,r}(0, \mathbf{x}_K)$ 
2: for  $k \in \{K-1, \dots, 1\}$  do
3:    $\mathbf{h}_k \leftarrow h_{\phi,r}(\mathbf{h}_{k+1}, \mathbf{x}_k)$   $\triangleright$  recurrence
4:    $\mathbf{A}_k \leftarrow h_{\phi,o_1}(\mathbf{h}_k, \mathbf{h}_{k+1})$   $\triangleright$  output
5: end for
6:  $\{\hat{\mu}_0, \hat{\Sigma}_0\} \leftarrow h_{\phi,o_2}(\mathbf{h}_1)$   $\triangleright$  output
7: return  $\{\hat{\mu}_0, \hat{\Sigma}_0, \mathbf{A}_{[0,T]}\}$ 
```

---

---

**Algorithm 3** Training of Adaptive Path Integral Autoencoder

---

**Input:** Dataset of observation sequences,  $\mathcal{D} = \{\mathbf{x}_{1:K}^{(i)}\}_{i=1, \dots, N}$ .

Latent and observation models,  $\mathbf{f}(\mathbf{z})$ ,  $\sigma(\mathbf{z})$ ,  $p_0(\mathbf{z})$  and  $p(\mathbf{x}|\mathbf{z})$ , parameterized by  $\theta$ .

Backward RNN as an inference network  $h_\phi : \mathbf{x}_{1:K} \rightarrow \{\hat{\mu}_0, \hat{\Sigma}_0, \mathbf{A}_{[0,T]}\}$ , parameterized by  $\phi$ .

```
1: while not  $\text{Converged}()$  do
2:   Sample datapoint  $\mathbf{x}_{1:K}$  from  $\mathcal{D}$ 
3:   Initialize  $\{\hat{\mu}_0, \hat{\Sigma}_0, \mathbf{A}_{[0,T]}\} \leftarrow h_\phi(\mathbf{x}_{1:K})$   $\triangleright$  Algorithm 2
4:    $\{\mathbf{z}_{[0,T]}, S_{\mathbf{u}}, \hat{w}\}^{1:L} \leftarrow \text{PI-ADAPTATION}(\hat{\mu}_0, \hat{\Sigma}_0, \mathbf{A}_{[0,T]}, \mathbf{x}_{1:K})$   $\triangleright$  Algorithm 1
5:    $\hat{\mathcal{L}} = \log \frac{1}{L} \sum_l \exp(-S_{\mathbf{u}}^{(l)})$ ,  $\nabla_{(\theta, \phi)} \hat{\mathcal{L}} \leftarrow - \sum_l \hat{w}^{(l)} \nabla_{(\theta, \phi)} S_{\mathbf{u}}^{(l)}$ 
6:   Update  $\theta$  and  $\phi$  with  $\nabla_{(\theta, \phi)} \hat{\mathcal{L}}$  using SGD  $\triangleright$  gradients are aggregated across mini-batches.
7: end while
```

---

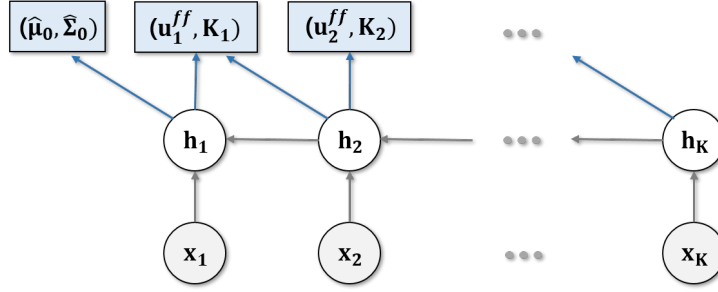


Figure 3: Structured inference network

## C Algorithmic Details

The pseudo code of APIAE training is shown in Algorithm 3. Given the observation data, the inference network implemented by the backward RNN first approximates the posterior distribution using Algorithm 2 (line 2–3). Then, the algorithm iteratively refines the variational distribution using path integral adaptation method in Algorithm 1 (line 4), estimates the lower bound of data likelihood and its gradients (line 5), and updates the model parameter according to the MCO gradients (line 6). The path integral adaptation and the MCO construction steps of APIAE can be seen as encoding and decoding procedures of autoencoders, respectively, motivating the name “adaptive path integral autoencoder.”

## D Experimental Details

### D.1 Pendulum

A 2-dimensional latent space was used and the locally-linear transition model used in Karl et al. [2017] were used, where the system dynamics were represented by combination of 16 linear systems as  $\mathbf{f}_\theta = \sum_{i=1}^{16} \alpha^{(i)} (A^{(i)} \mathbf{z} + c^{(i)})$ ,  $\sigma = \sum_{i=1}^{16} \alpha^{(i)} B^{(i)}$  and  $\alpha = f_\lambda(\mathbf{z}) \in \mathbb{R}^{16}$  is a single layer neural network having 16 softmax outputs parameterized by  $\lambda$ , i.e.,  $\{A^{(i)}, B^{(i)}, c^{(i)}, \lambda\} \subset \theta$ . For the stochastic simulation, we simply chose  $t_k = (k - 1)\delta t$ , and  $\delta t = T/(K - 1)$ . For the observation model, we considered a neural network with Gaussian outputs as  $p(\cdot|\mathbf{z}) = \mathcal{N}(\cdot; \mu_\theta(\mathbf{z}), \sigma_\theta(\mathbf{z}))$ , where  $\mu_\theta(\cdot)$  and  $\sigma_\theta(\cdot)$  are outputs of a neural network having 1a single hidden layer of 128 hidden units with ReLU activation and a  $2 \times 256$ -dimensional output layer without activation. We found that initializing dynamics network as stable results in the more stable learning, so the dynamics network was initialized with the supervised learning with transition data from stable linear system.

### D.2 Human Motion Capture Data

A 3-dimensional latent state space was used in this example and the dynamics were parameterized by the locally-linear transition model as in the pendulum experiment. The system dynamics were represented by combination of 16 linear systems as  $\mathbf{f}_\theta = \sum_{i=1}^{16} \alpha^{(i)} (A^{(i)} \mathbf{z} + c^{(i)})$ ,  $\sigma = \sum_{i=1}^{16} \alpha^{(i)} B^{(i)}$  and  $\alpha = f_\lambda(\mathbf{z}) \in \mathbb{R}^{16}$  is a single layer neural network having 16 softmax outputs parameterized by  $\lambda$ , i.e.,  $\{A^{(i)}, B^{(i)}, c^{(i)}, \lambda\} \subset \theta$ . For the stochastic simulation, we simply chose  $t_k = (k - 1)\delta t$ , and  $\delta t = T/(K - 1)$ . For the observation model, we considered a neural network with Gaussian outputs as:  $p(\cdot|\mathbf{z}) = \mathcal{N}(\cdot; g_\theta(\mathbf{z}), I_{62})$ , where  $g_\theta(\cdot)$  is a neural network having a single hidden layer of 128 hidden units with ReLU activation and a 62-dimensional output layer without activation.

### D.3 Additional Results

To investigate the optimal parameters for APIAE training, we varied parameters of APIAEs, i.e.,  $L$ ,  $R$ ,  $K$ , and compared the results.

<sup>3</sup>At the first iteration,  $\bar{\mathbf{u}}^{ff}(t)$ ,  $\bar{\mathbf{K}}(t)$  and  $q_0$  are obtained from the inference network and  $\bar{\mu}(t) = 0$ ,  $\bar{\Sigma}(t) = I$ .



Table 2: The lower bound of log-likelihood for models trained with APIAEs w.r.t. the sample size.

|         | Pendulum ( $\times 10^6$ ) |         |         |         | Mocap ( $\times 10^5$ ) |        |        |        |
|---------|----------------------------|---------|---------|---------|-------------------------|--------|--------|--------|
|         | L=4                        | L=8     | L=16    | L=64    | L=4                     | L=8    | L=16   | L=64   |
| APIAE+r | -9.9282                    | -9.8380 | -9.8322 | -9.8306 | -6.689                  | -6.665 | -6.637 | -6.683 |
| APIAE   | -9.9724                    | -9.9318 | -9.9153 | -9.8552 | -6.689                  | -6.680 | -6.661 | -6.629 |

Table 3: The lower bound of data log-likelihood for models trained with APIAEs w.r.t. the number of path-integral adaptations.

|         | Pendulum ( $\times 10^6$ ) |        |        | Mocap ( $\times 10^5$ ) |        |        |
|---------|----------------------------|--------|--------|-------------------------|--------|--------|
|         | R=0                        | R=4    | R=8    | R=0                     | R=4    | R=8    |
| APIAE+r | -9.890                     | -9.866 | -9.795 | -6.687                  | -6.665 | -6.648 |
| APIAE   | -9.974                     | -9.927 | -9.929 | -6.683                  | -6.680 | -6.669 |

Table 2 and Table 3 show the lower bounds of APIAEs for two experiments by varying the number of samples  $L$  and adaptation  $R$ , respectively. As shown in the result, higher lower bound is achieved as the number of samples and adaptation get larger. Note, however, that APIAEs become computationally expensive as those parameters increase and slow down the training speed. Thus, we need to look for the compromise between the training efficiency and the performance. Empirically found that  $L = 8$  and  $R = 4$  show a reasonable performance with computational efficiency.

Fig. 4 show the learning results for the dataset of difference time length. It is observed that, when the observations are highly-noisy, the learning algorithm fails to extract enough temporal information from the data and then fails to build a valid generative dynamical model.

The lower bound of learned models are reported in Table 4 and Fig. 5. As in the Table 4, the highest lower bounds were achieved by the APIAE algorithms. Thus, the learning performances are seen to be improved via adaptation procedures with training on any bound. We also found that APIAEs produce higher bound than FIVO or IWAE throughout the training stage as shown in the Fig. 5.

Finally, Fig. 7 depicts the additional results of the Mocap experiment for the learned latent space, reconstruction, and prediction.

Table 4: Comparison of APIAE, FIVO, and IWAE bounds in the pendulum experiment. Each model was trained with (i) APIAE with resampling (+r), (ii) APIAE without resampling, (iii) FIVO, and (iv) IWAE. The resulting APIAE, FIVO, and IWAE bounds are shown.

|         | Pendulum ( $\times 10^6$ ) |               |         |         | Mocap ( $\times 10^5$ ) |               |        |        |
|---------|----------------------------|---------------|---------|---------|-------------------------|---------------|--------|--------|
|         | APIAE+r                    | APIAE         | FIVO    | IWAE    | APIAE+r                 | APIAE         | FIVO   | IWAE   |
| APIAE+r | <b>-9.866</b>              | -10.213       | -9.902  | -10.308 | <b>-6.665</b>           | -6.694        | -6.683 | -6.723 |
| APIAE   | -10.020                    | <b>-9.927</b> | -10.037 | -9.953  | -6.712                  | <b>-6.680</b> | -6.739 | -6.707 |
| FIVO    | <b>-9.868</b>              | -10.145       | -9.890  | -10.197 | <b>-6.675</b>           | -6.691        | -6.687 | -6.711 |
| IWAE    | -9.998                     | <b>-9.959</b> | -10.145 | -9.974  | -6.694                  | <b>-6.668</b> | -6.706 | -6.683 |

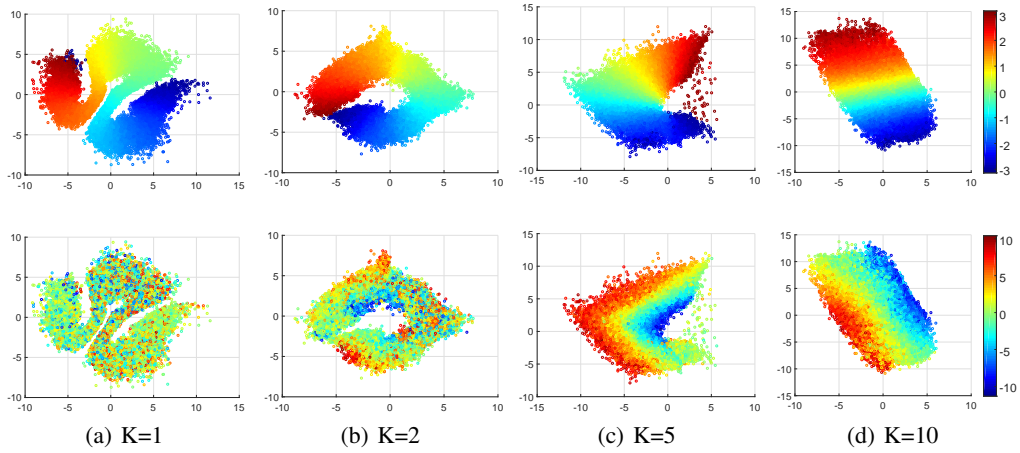


Figure 4: Pendulum experiment. The learned latent space colored by (top) angles and (bottom) angular velocities of the ground truth for different dataset with varying length,  $K = 1, 2, 5, 10$ .

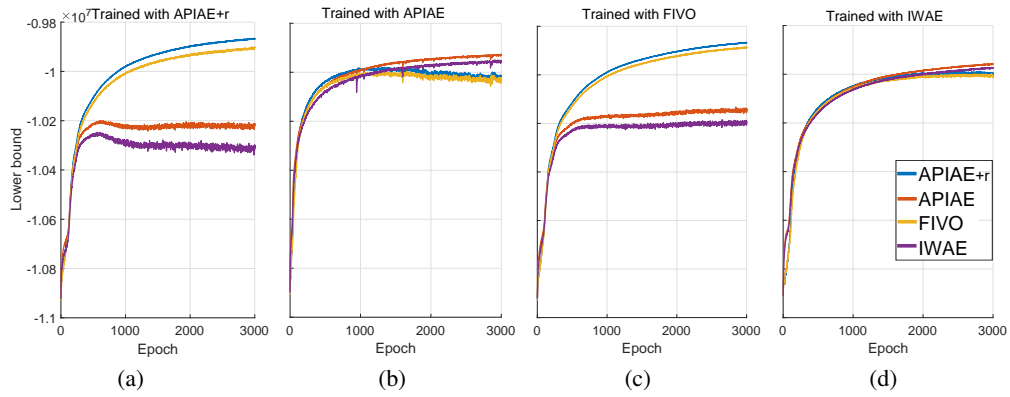


Figure 5: Comparison of APIAE, FIVO, and IWAE bounds in the pendulum experiment. For each model trained with (a) APIAE with resampling, (b) APIAE without resampling, (c) FIVO, and (d) IWAE, the APIAE, FIVO, and IWAE bounds are shown.

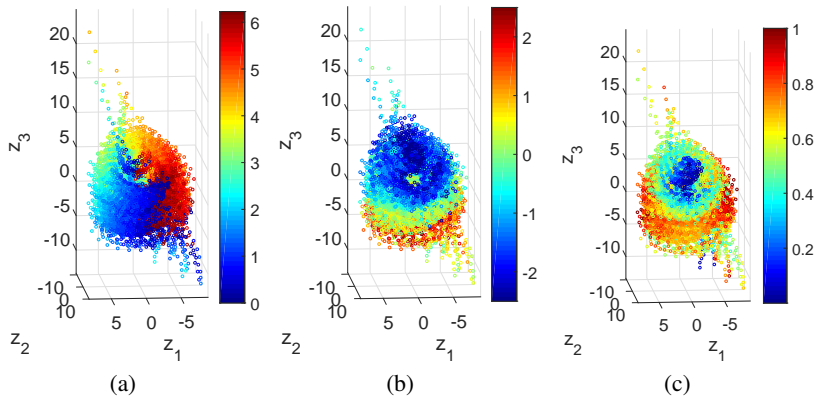
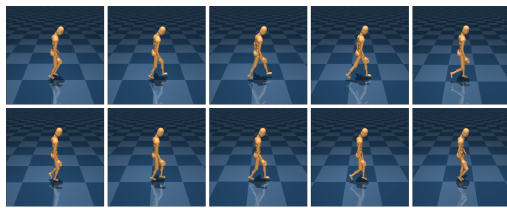
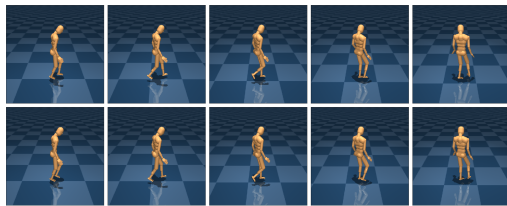


Figure 6: Mocap experiment. The learned latent space colored by (a) the gait phase, (b) yaw rate, and (c) forward velocity of the ground truth in another view.



(a)



(b)



(c)

Figure 7: (a-b) Locomotion reconstruction results. Top: ground truth, Bottom: reconstruction. (c) Prediction results from the same initial pose.